scientific reports

Check for updates

OPEN

Hybrid quantum-classical stochastic programming for co-planning 5G base stations and photovoltaic power stations in urban communities

Yue Xu, Xutao Han, Renjie Luo & Zhiyi Li✉

The rapid deployment of Fifth-generation base stations (5G BSs) in urban communities has led to rising electricity costs for mobile network operators. Meanwhile, distributed photovoltaic power plants (PVs) provide a promising solution to offset energy expenses and reduce renewable energy curtailment. This study proposes a hybrid quantum-classical two-stage stochastic programming approach for the co-planning of BSs and PVs in urban communities. In the first stage, warm-start quantum annealing is employed to determine BS deployment locations and capacities. In the second stage, data envelopment analysis (DEA) is used to evaluate and improve the operational performance of the integrated BS-PV system. Case study results show that the proposed method reduces total planning costs to one-third compared to traditional experience-based strategies, enhances PV utilization by 12.53%, reduces electricity costs by 51.04%, and achieves over 5.4 times improvement in computational efficiency. These results demonstrate not only technical advantages but also practical value in supporting cost-effective and low-carbon urban infrastructure planning.

Keywords 5G base station, Two-stage stochastic programming, Quantum-classical hybrid framework, Quantum annealing, Data envelope analysis

With the rapid development and widespread application of big data, artificial intelligence, and the Internet of Things, telecoms have assumed an increasingly pivotal role across various fields. Fifth-generation base stations (5G BSs), as central hubs for information transmission in this digital revolution[1], are extensively deployed in urban communities by mobile network operators (MNOs) to offer higher transmission rates and lower latency[2]. The effective deployment of 5G BSs demands a comprehensive approach that integrates telecoms quality, energy provisioning, and construction expenditures, rather than a simple replacement of legacy infrastructure. On the one hand, the total energy consumption of a 5G BS can be up to three times higher than that of an existing 4G BS, while its coverage area is only about 20% of that of a 4G base station[3,4], thus rendering traditional planning approaches inadequate as they often place significantly greater emphasis on the quality of telecom service than on energy consumption. On the other hand, modern power systems now feature higher penetrations of photovoltaic power plants (PVs), offering increased flexibility in energy supply[5,6]. The deployment of a 5G BS cluster not only focuses on the construction cost but also furnishes the potential for power system dispatching, while the operation scheme about the accessorial energy storage (ES) and air conditioning (AC) further enlarges the PV utilization[7]. Thus, reasonable deployment and operation are significant for both the MNO and the distribution network operator (DNO).

A typical urban community is presented in Fig. 1, in which MNO and DNO plan to collaboratively deploy a new 5G BS cluster to address the increasing telecom demands for efficiency. Additionally, they aim to jointly develop an operation scheme that minimizes operation cost and traditional energy consumption by maximizing PV utilization[8]. The decision objects of this optimization problem include BS and PV clusters, making it a typical problem with a bilateral-matching framework[9]. The process involved in this problem encompasses deployment and operation performance evaluation, in which the decision objects in the deployment stage are only related to the BS cluster since the PV cluster has been constructed and fixed beforehand, and operation performance evaluation involves the hybrid optimization of both BS and PV clusters. The scale of an urban community is

College of Electrical Engineering, Zhejiang University, Hangzhou, China. ✉email: zhiyi@zju.edu.cn

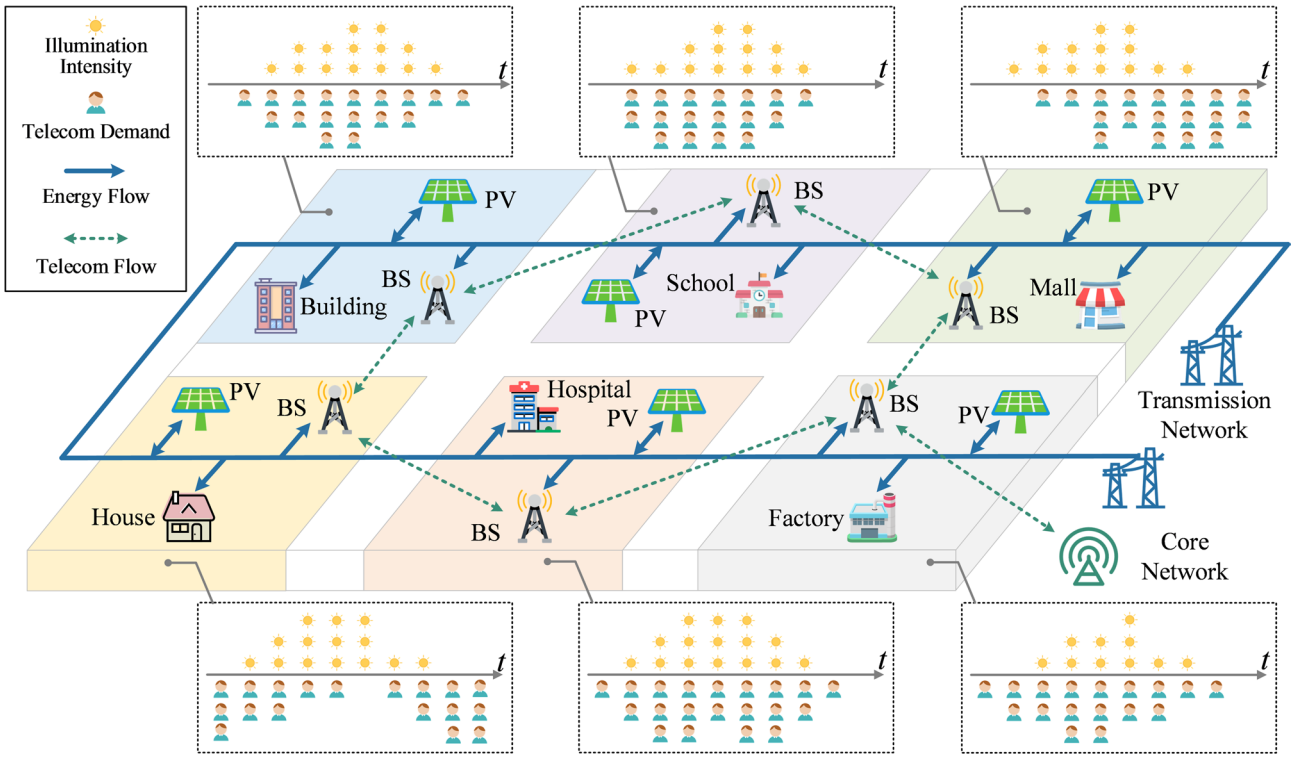

Fig. 1. Formation of a typical urban community. The BS and PV clusters in the urban community are strategically deployed across subareas. Each subarea's telecom demand (BS power consumption) follows typical scenario patterns. PV outputs also show spatial regularity and partial predictability. During off-peak periods, BS clusters can be self-sufficient, while during peak times, they rely on a mix of PVs, the grid, and local ES units, with predictable contributions due to clustering effects.

typically determined by factors such as geographical area and population density, with the number of nodes ranging from several dozen to several hundred. More importantly, each unit within a BS requires independent design and regulation across massive typical scenarios to achieve an optimal deployment and operation scheme[10]. This significantly multiplies the decision variables, often reaching into the hundreds or more. While the physical scale of an urban community may not be large, the mathematical model is quite tremendous, and the computational complexity of classical algorithms grows exponentially. As urban communities continue to expand, the number of factors involved in planning increases rapidly. As a result, the planning process faces an overwhelming demand for computational time and resources due to the curse of dimensionality, which is an unsustainable challenge for operators.

Current research concerning the deployment and operation performance presents certain limitations, leading to a gap between the problem framework and application. For instance, most BS-focused research primarily targets the optimization of BS operation[11–13], load migration[14,15], or ES configurations[4,16] as individual objectives. Alternatively, in PV-focused studies, BS clusters are typically treated as loads for demand response within the power system scheduling framework[17]. However, few studies address the planning problem holistically, considering MNO and DNO as a shared community of interest. The main challenge lies in the significant computational burden introduced by such a complex framework, which involves numerous variables, nonlinear constraints, and intertwined uncertainties from both supply and demand. These factors collectively strain the capabilities of conventional algorithms. Recent research efforts primarily address these challenges through improvements in frameworks[18–21], algorithm enhancements[22–24], and efficient representations of uncertainty[25–28], with their contributions and limitations summarized in Table 1. Overall, existing deployment and operation methods still have room for improvement in both accuracy and computational efficiency.

As an emerging technique, quantum annealing (QA) has shown superiority in dealing with combinatorial optimization problems in terms of energy management of power systems, such as unit commitment[29,30], network reconfiguration[31,32], and economic dispatch[33,34]. The matching of binary combinatorial variables with the two-state qubits also presents a promising opportunity for leveraging QA in BS deployment, which is not only theoretically feasible but also holds practical significance. However, QA is currently hindered by limitations in hardware performance, which constrain its computational scale[35]. Furthermore, its inability to natively process continuous variables significantly hampers its effectiveness in tackling complex operation problems that involve power-related variables. To mitigate these challenges, the warm-starting technique and data envelopment analysis (DEA) executed on classical computing platforms are proposed as assistance to operation efficiency evaluation[36]. Warm-starting technology enhances annealing performance by providing a better initial solution to the QA, thereby improving the optimization scales and convergence rates. Concurrently, DEA can be

Categories	Methods	Contributions	Insufficiencies
Framework Improvement	Stackelberg Game[18]	Decomposition of the original problem into multiple subproblems	Computational burden increases exponentially with problem scale
	SESSION[19]	Two-stage co-planning of ES capacity and operation scheme	
	Robust-CVaR[20]	Hybrid CVaR robust risk modeling for stochastic optimization	
	JSSP Model[21]	MILP model for optimal joint switching mechanism	
Algorithm Enhancement	NSGA-II[22]	Optimization of 5G BSs participating in VPP scheduling	Interpretability is weak, and accuracy is reduced as problem complexity increases
	PSO[23]	Optimization of 5G BSs deployment	
	Power Aggregation Simplification[24]	Mobile network optimization with power aggregation	
Uncertainty Representation	ARMA+BAVOA[25]	ARMA-based wind power prediction	Computational complexity increases with the number of scenarios
	Stochastic Distribution Model[26]	Time-correlated random distributions in stochastic optimization	
	Random Model of Meteorology[27]	Efficient scenario aggregation	
	IGDT[28]	IGDT-based optimal bidding strategy	

Table 1. Taxonomy of literature addressing complex deployment and operation problems.

employed to address complexities associated with continuous variables, offering a complementary approach that capitalizes on classical computational strengths.

In this context, a hybrid quantum-classical stochastic programming framework is proposed for the deployment and operation performance evaluation to optimize the joint interests of MNO and DNO. This framework accounts for the stochasticity of BS loads and PV outputs, representing them through massive typical scenarios and their associated probability distributions. The co-planning process in this framework is divided into two stages: In the first stage, the problem addresses the location and type selection of BSs for MNO. Building on this, DNO provides operation schemes to MNO at minimal cost while utilizing the adjustable capabilities of BSs to enhance PV utilization in the second stage. This is achieved by precisely matching source and load models across a large set of scenarios, thereby fostering a win-win collaboration between the two agents. Given that the combinatorial optimization problem is NP-Hard[37], a warm-starting quantum annealing (WSQA) technique and DEA are introduced to develop a more efficient algorithm for solving the stochastic programming problem.

Compared to the methods listed in Table 1, the proposed approach in this study effectively balances computational accuracy and efficiency. The innovations of this work lie in the following aspects:

1) A hybrid quantum-classical two-stage stochastic programming framework is proposed for BS-PV integrated urban communities. This framework efficiently coordinates deployment and operation by leveraging quantum annealing for the planning stage and classical optimization for the operation stage, aiming to develop more effective strategies compared to traditional frameworks.
2) A quantum annealing algorithm enhanced with warm-starting techniques is employed to develop the deployment scheme for the BS cluster, significantly improving computational accuracy and efficiency while enabling scalability for large-scale mixed-integer programming problems.
3) A DEA-based operation optimization is introduced to avoid complex nonlinear constraints in massive scenarios. This method enables the identification of optimal operation schemes that maximize performance metrics and improve PV utilization.

Methods

Framework for hybrid stochastic programming

Quantum annealing can greatly enhance the computational efficiency of problems involving binary variables, such as BS deployment[38]. However, the inherent limitations make it inferior in handling problems with continuous variables, such as operation performance evaluation. Therefore, the proposed hybrid quantum-classical stochastic programming framework is structured into two sequential stages, as illustrated in Fig. 2.

The first-stage problem, aiming to locate the BSs and set the specifications of their TD, ES, and AC units under the constraints of the telecommunication quality with a fixed capacity of BSs in a cluster, is solved by WSQA since it is dominated by binary variables. The selected deployment solution defines a set of DMUs, which are then passed as inputs to the second stage. The second-stage problem focuses on the operation schemes considering the massive scenarios of loads and outputs in BS-PV integrated urban communities, in which the operation and electricity costs are regarded as investments, and four decision-making indices are selected to evaluate the effectiveness. This problem involves a large number of continuous operational indices; thus is addressed using DEA running on conventional computers to perform efficient numerical computation. The interaction between the two stages ensures that both strategic infrastructure planning and tactical operation management are co-optimized within a unified stochastic programming model. This design enables the framework to handle large-scale, uncertain scenarios while maintaining computational tractability and practical interpretability. A more detailed explanation of the proposed model and method within this framework is provided in the supplemental information.

Uncertainty representation

To address the uncertainty in BS-PV co-planning, a scenario-based modeling approach is adopted. Typical scenarios are generated based on key external factors, such as typical day types (D_{BS}), ambient temperature (T_{BS}), seasons (S_{PV}), and weather (W_{PV}), which significantly affect BS demands and PV outputs. These factors are

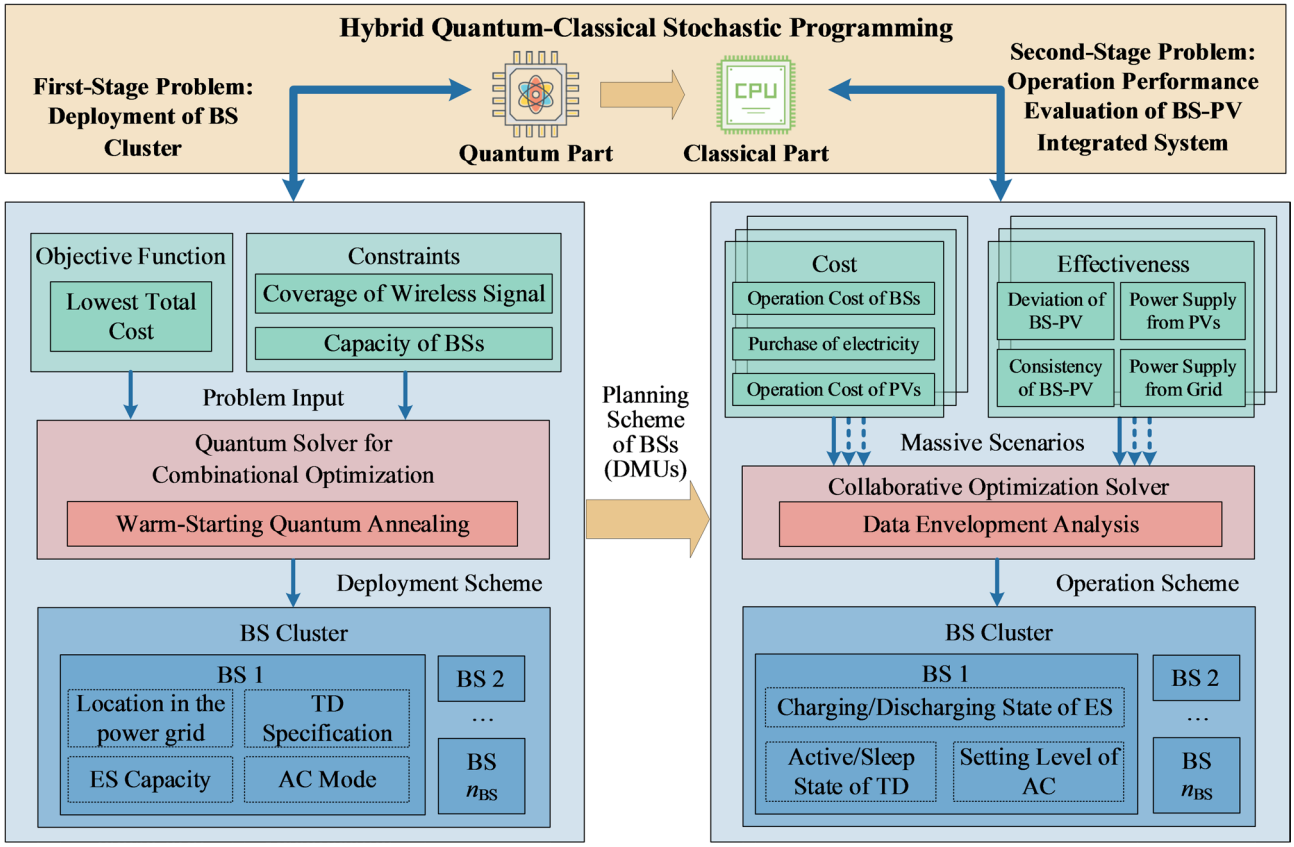

Fig. 2. Framework for the two-stage stochastic programming of BS-PV integrated urban communities. The framework includes deployment and operation performance evaluation stages: the first locates BSs and configures TD, ES, and AC units under telecom constraints; the second optimizes operation under multiple scenarios, using four indices to evaluate cost-effectiveness.

Enumeration	D_{BS}	T_{BS} (℃)	S_{PV}	W_{PV}
1	Weekday	T_{BS}<10	Spring, Autumn	Sun
2	Day Off	10≤T_{BS}<25	Summer	Cloud
3	Holiday	T_{BS}≥25	Winter	Others

Table 2. Simplified scenarios and their clustered enumerations

abstracted into indicators derived from historical data. For instance, BSs near malls show peak load on holidays, PV output varies seasonally due to solar radiation, and ambient temperature impacts the air-conditioning energy of BSs.

Computational efficiency is improved while preserving representativeness by clustering similar scenarios using reduction techniques such as K-means. For example, PV outputs in spring and autumn are merged, and extreme weather types are grouped. Sequential scenarios are then generated via permutation of simplified indicators, excluding implausible combinations (e.g., high temperature in winter). These sequences, along with their associated probabilities, form the basis for uncertainty-aware optimization of the BS-PV configuration model. Table 2 lists the indicators and ranges of each simplified scenario.

In order to fully represent the external environment, simplified scenarios are combined into sequential scenarios through permutation, as shown in Fig. 3. Based on historical data, each sequential scenario yields BS load and PV output curves with corresponding deviation distributions. These sequences are assumed to be independent and identically distributed, forming the uncertainty of the optimization model.

QA for combinatorial optimization

The objective function in the first-stage problem is related to the total cost in the construction and operation stages as:

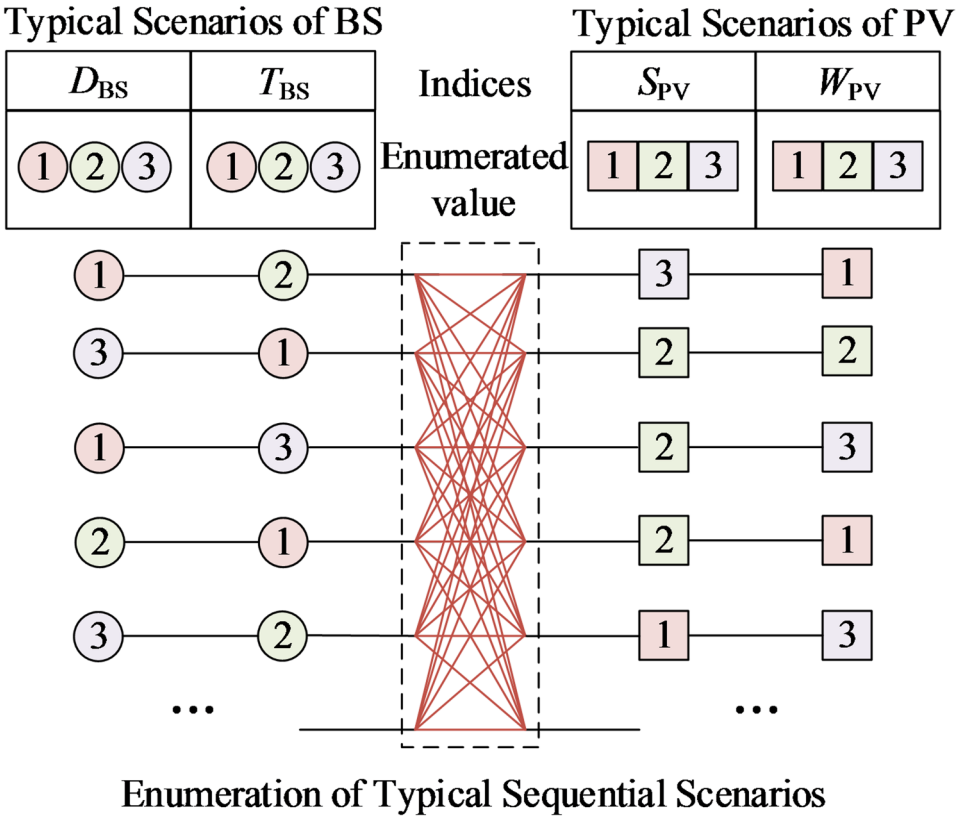

Fig. 3. Permutations and combinations of the typical scenarios. Unlikely combinations (e.g., high temperature in winter with T_{BS}=S_{PV}=3) are excluded to reduce the number of sequential scenarios.

$$\min C = \sum_{i=1}^{n_{BS}} c_{sum,i} u_i = \sum_{i=1}^{n_{BS}} (c_{cns,i} + c_{TD} \sum_{j=1}^{n_{TD}} v_{TD,i,j} + c_{ES} \sum_{k=1}^{n_{ES}} v_{ES,i,k} + c_{AC} \sum_{l=1}^{n_{AC}} v_{AC,i,l}) u_i \quad (1)$$

The constraints in the model of the first-stage problem include the requirements of the BS capacity (Eq. (2)), coverage[39] (Eq. (3)), and the interdependence among the selected specifications of the TD, ES, and AC units (Eqs. (4)–(5)):

$$k_{cp} \sum_{j=1}^{n_{TD}} u_i v_{TD,i,j} = R_{BS,i}, \forall i \in n_{BS} \quad (2)$$

$$(d_i + d_j) u_i u_j \leqslant L_{ij}, \forall i, j \in n_{BS} \quad (3)$$

$$\sum_{j=1}^{n_{TD}} v_{TD,i,j} + \sum_{j=1}^{n_{AC}} v_{AC,i,j} = \sum_{j=1}^{n_{ES}} v_{ES,i,j} \quad (4)$$

$$\sum_{i=1}^{n_{BS}} u_i = M_{BS}, \sum_{i=1}^{n_{BS}} \sum_{j=1}^{n_{TD}} v_{TD,i,j} = M_{TD}, \sum_{i=1}^{n_{BS}} \sum_{j=1}^{n_{ES}} v_{ES,i,j} = M_{ES}, \sum_{i=1}^{n_{BS}} \sum_{j=1}^{n_{AC}} v_{AC,i,j} = M_{AC} \quad (5)$$

QA leverages adiabatic evolution within the D-Wave quantum annealer[40] to enhance efficiency and accuracy in finding optimal solutions, primarily through its unique quantum tunneling effect[41,42]. It requires Eqs. (1)–(5) be reformulated into a quadratic unconstrained binary optimization (QUBO) form[43] so as to establish a mapping between the objective function and the Hamiltonian energy function[44]. The QUBO-based optimization model is designed as follows, in which all decision variables are restricted to binary values, and no explicit constraints are present[45]:

$$\min C_{\mathrm{QUBO}} = \sum_{i=1}^{n_{\mathrm{BS}}} c_{\mathrm{sum},i} u_i + \rho_1 (k_{\mathrm{cp}} \sum_{j=1}^{n_{\mathrm{TD}}} u_i v_{\mathrm{TD},i,j} - R_{\mathrm{BS},i})^2 + \rho_2 [L_{ij} - (d_i + d_j) u_i u_j + \xi]^2 + \rho_3 (\sum_{j=1}^{n_{\mathrm{TD}}} v_{\mathrm{TD},i,j} + \sum_{j=1}^{n_{\mathrm{AC}}} v_{\mathrm{AC},i,j} - \sum_{j=1}^{n_{\mathrm{ES}}} v_{\mathrm{ES},i,j})^2$$
$$+\rho_4 (\sum_{i=1}^{n_{\mathrm{BS}}} u_i - M_{\mathrm{BS}})^2 + \rho_5 (\sum_{i=1}^{n_{\mathrm{BS}}} \sum_{j=1}^{n_{\mathrm{TD}}} v_{\mathrm{TD},i,j} - M_{\mathrm{TD}})^2 + \rho_6 (\sum_{i=1}^{n_{\mathrm{BS}}} \sum_{j=1}^{n_{\mathrm{ES}}} v_{\mathrm{ES},i,j} - M_{\mathrm{ES}})^2 + \rho_7 (\sum_{i=1}^{n_{\mathrm{BS}}} \sum_{j=1}^{n_{\mathrm{AC}}} v_{\mathrm{AC},i,j} - M_{\mathrm{AC}})^2 \quad (6)$$

where

$$c_{\mathrm{sum},i} = c_{\mathrm{cns},i} + c_{\mathrm{TD}} \sum_{j=1}^{n_{\mathrm{TD}}} v_{\mathrm{TD},i,j} + c_{\mathrm{ES}} \sum_{k=1}^{n_{\mathrm{ES}}} v_{\mathrm{ES},i,k} + c_{\mathrm{AC}} \sum_{l=1}^{n_{\mathrm{AC}}} v_{\mathrm{AC},i,l} \quad (7)$$

The following equation illustrates the specific discretized process for the continuous variable ξ:

$$\xi = \sum_{a=0}^{n_1} 2^a z_i^{\xi} + \sum_{b=1}^{n_2} 2^{-b} z_{n_1+b}^{\xi} \quad (8)$$

After formulating the objective function in QUBO form, the quantum annealer executes the QA algorithm through the following steps:

1) minor embedding: The problem graph is mapped onto the physical qubit architecture (e.g., D-Wave's Chimera or Pegasus) using a minor embedding algorithm to fit the hardware constraints.

2) quantum initialization: The system is initialized in a quantum superposition of all possible states via a transverse magnetic field, enabling exploration of the entire solution space. A warm-starting technology is introduced in this stage to speed up the subsequent process.

3) adiabatic evolution: The system Hamiltonian is gradually evolved from a simple initial form to the problem Hamiltonian. During this process, the system tends toward lower energy configurations.

4) quantum tunneling: Quantum effects such as tunneling allow the system to escape local minima and explore globally optimal solutions more effectively than classical heuristics.

5) solution readout: After the annealing process, the system collapses into a low-energy (ideally optimal) state, which is read out as the final solution.

Warm-starting technology

A warm-starting technology is introduced to enhance the computational efficiency of the QA algorithm, in which a classical computer is employed to pre-solve the master problem and fix the values of certain variables based on the characteristics of feasible solutions[46].

In the first step, n sets of feasible solutions to the master problem, which are represented in the following matrix form as [$\boldsymbol{X}$p 1, $\boldsymbol{X}$p 2,…, $\boldsymbol{X}$p n]$^{\mathrm{T}}$ in Eq. (9):

$$\boldsymbol{X}^{\mathrm{p}} = \begin{bmatrix} \boldsymbol{X}_1^{\mathrm{p}} \\ \boldsymbol{X}_2^{\mathrm{p}} \\ \vdots \\ \boldsymbol{X}_n^{\mathrm{p}} \end{bmatrix} = \begin{bmatrix} x_{1,1}^{\mathrm{p}} & x_{1,2}^{\mathrm{p}} & \cdots & x_{1,m}^{\mathrm{p}} \\ x_{2,1}^{\mathrm{p}} & x_{2,2}^{\mathrm{p}} & \cdots & x_{2,m}^{\mathrm{p}} \\ \vdots & \vdots & \ddots & \vdots \\ x_{n,1}^{\mathrm{p}} & x_{n,2}^{\mathrm{p}} & \cdots & x_{n,m}^{\mathrm{p}} \end{bmatrix} \quad (9)$$

On this basis, each x_j is allocated to one of two sets: X^{d}, which includes pre-fixed variables, or X^{v}, which contains the variables that need to be solved. The boundary between these sets is determined by analyzing the distribution of feasible solutions, as outlined as follows:

$$x_j \in \begin{cases} \boldsymbol{X}^{\mathrm{d}} & \left| \sum_{i=1}^{n} x_{i,j}^{\mathrm{p}} - \frac{n}{2} \right| > \varepsilon_1 \\ \boldsymbol{X}^{\mathrm{v}} & \left| \sum_{i=1}^{n} x_{i,j}^{\mathrm{p}} - \frac{n}{2} \right| \leqslant \varepsilon_1 \end{cases}, j \in [1, m] \quad (10)$$

The elements in the set X^{d} are pre-fixed according to the highest probability of occurrence in the feasible solutions as follows:

$$x_j = \begin{cases} 0 & P(x_{i,j}^{\mathrm{p}} = 0) \geqslant P(x_{i,j}^{\mathrm{p}} = 1) \\ 1 & P(x_{i,j}^{\mathrm{p}} = 0) < P(x_{i,j}^{\mathrm{p}} = 1) \end{cases}, x_j \in X^{\mathrm{d}} \quad (11)$$

The variables in the set X^{v} are input into a quantum annealer with a tentative initial state generated based on ε_2, while a total of m_d elements contained in X^{d} are input as fixed values instead of variables, which reduces the variable size of the master problem from m to m-m_d and achieves a convergence rate superior to that of the original algorithm[47]. A flowchart visualizing the above warm-starting process through a three-variable case is shown in Fig. 4.

DEA-assisted operation performance evaluation

DEA is a non-parametric method that constructs a production possibility frontier using DMUs' input-output data to assess their relative efficiency. When it comes to the proposed second-stage problem with multiple inputs

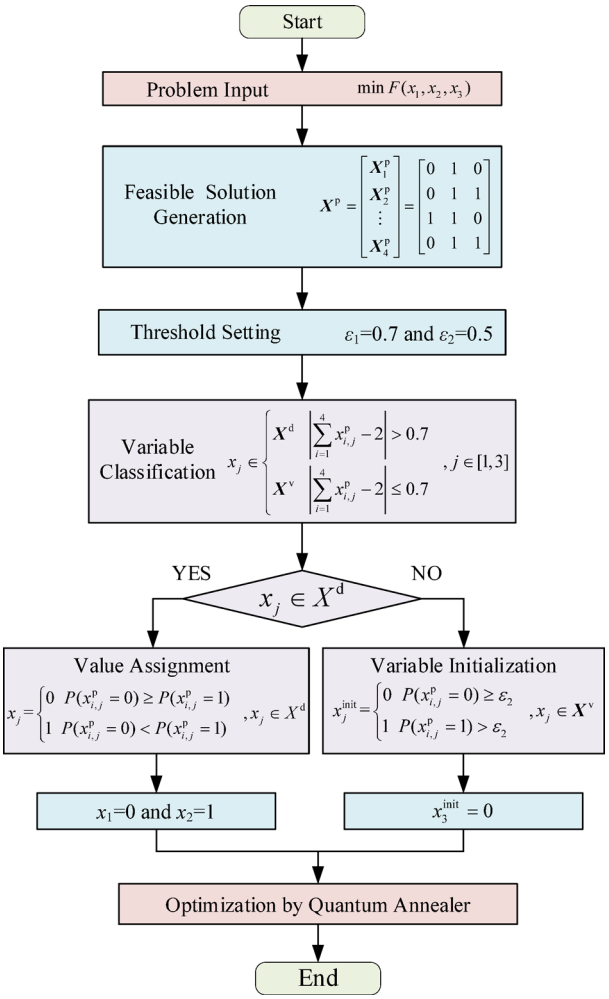

Fig. 4. Flowchart of the warm-starting process through a three-variable case. Red boxes show inputs/outputs, blue boxes denote variable assignments, and purple boxes represent key warm-starting steps.

and outputs from massive scenarios, DEA can be used for evaluation and decision-making[48], in which the specific BSs achieved by the first-stage problem are viewed as DMUs.

According to the bilateral-matching theory[49], DEA adopts four indices to evaluate the effectiveness of the operation scheme. *DI* captures the discrete supply-demand deviation between BSs and PVs based on bilateral matching, while *CI* complements it with a continuous measure. To assess cost-effectiveness, *PR* and *GR* are introduced from two opposite perspectives, reflecting PV utilization and BS dependency. Due to the stochasticity of BSs and PVs, all indices are formulated as expected values, as shown below.

$$\mathrm{E}_S(DI) = \sum_{s=1}^{S} \mathbf{D}_s = \sum_{s=1}^{S} \sum_{t=1}^{T} \eta_{s,t} [\sum_{j \in \mathrm{G_{PV}}} (P_{j,s,t}^{\mathrm{PV}} - P_{\mathrm{L},j,s,t}^{\mathrm{PV}}) - \sum_{i \in \mathrm{G_{BS}}} P_{\mathrm{BS},i,s,t}^{\mathrm{PV}}] \tag{12}$$

$$\mathrm{E}_S(CI) = \frac{\sum_{s=1,}^{S} \sum_{t=1}^{T} \Delta P_{\mathrm{BS},s,t}^{\mathrm{PV}} \Delta P_{s,t}^{\mathrm{PV}}}{\sqrt{\sum_{s=1,}^{S} \sum_{t=1}^{T} (\Delta P_{\mathrm{BS},s,t}^{\mathrm{PV}})^2 (\Delta P_{s,t}^{\mathrm{PV}})^2}} \tag{13}$$

$$\mathrm{E}_S(PR) = \frac{\sum_{s=1}^{S} \sum_{t=1}^{T} \sum_{i \in \mathrm{G_{BS}}} P_{\mathrm{BS},i,s,t}^{\mathrm{PV}}}{\sum_{s=1}^{S} \sum_{t=1}^{T} \sum_{i \in \mathrm{G_{BS}}} (P_{s,t}^{\mathrm{PV},j} - P_{\mathrm{L},s,t}^{\mathrm{PV},j})} \tag{14}$$

$$\mathrm{E}_S(GR) = \frac{\sum_{s=1}^{S}\sum_{t=1}^{T}\sum_{k\in \mathrm{G}_0} P_{\mathrm{BS},s,t}^{\mathrm{G},k}}{\sum_{s=1}^{S}\sum_{t=1}^{T}\sum_{k\in \mathrm{G}_0} P_{s,t}^{\mathrm{G},k}} \tag{15}$$

The expected values of these four indices are used as DEA outputs, while the following three cost-related terms, i.e., $C_{\mathrm{BS},i}$, $C_{\mathrm{E},i}$, and $C_{\mathrm{PV},i}$, denoting the operation cost of BSs, electricity cost, and PV curtailment penalty, are selected as inputs and expressed as follows.

$$C_{\mathrm{BS},i} = C_{\mathrm{ES}}^{\mathrm{M,avg}} R_{\mathrm{ES},i} + \sum_{s=1}^{S}\sum_{t=1}^{T} (C_{\mathrm{TD}}^{\mathrm{md}} w_{\mathrm{TD},i,s,t} + C_{\mathrm{ES}}^{\mathrm{md}} w_{\mathrm{ES},i,s,t} + C_{\mathrm{AC}}^{\mathrm{md}} w_{\mathrm{AC},i,s,t}) \tag{16}$$

$$C_{\mathrm{E},i} = C^{\mathrm{G}} \sum_{s=1}^{S}\sum_{t=1}^{T} P_{\mathrm{BS},i,s,t}^{\mathrm{G}} \tag{17}$$

$$C_{\mathrm{PV},i} = C^{\mathrm{penalty}} \sum_{s=1}^{S}\sum_{t=1}^{T} [\frac{1}{M_{\mathrm{BS}}} \sum_{j\in G_{\mathrm{PV}}} (P_{j,s,t}^{\mathrm{PV}} - P_{\mathrm{L},j,s,t}^{\mathrm{PV}}) - P_{\mathrm{BS},i,s,t}^{\mathrm{PV}}] \tag{18}$$

The original cost evaluation problem is divided and transformed into i optimization problems aiming at solving the maximum cost-effectiveness ratio according to the theory of DEA[50], which is expressed as follows:

$$\max \frac{\boldsymbol{X}^{\mathrm{T}}\boldsymbol{E}}{\boldsymbol{Y}^{\mathrm{T}}\boldsymbol{C}_i} = \frac{-x_1 \mathrm{E}_S(DI) + x_2 \mathrm{E}_S(CI) + x_3 \mathrm{E}_S(PR) - x_4 \mathrm{E}_S(GR)}{y_1 C_{\mathrm{BS},i} + y_2 C_{\mathrm{E},i} + y_3 C_{\mathrm{PV},i}} \tag{19}$$

$$\text{s.t. } \boldsymbol{X}^{\mathrm{T}}\boldsymbol{E} \leqslant \boldsymbol{Y}^{\mathrm{T}}\boldsymbol{C}_i \tag{20}$$

Given the complexity of solving this nonlinear optimization problem directly, the Charnes-Cooper transformation is applied to achieve linearization using the following mapping[51]:

$$\boldsymbol{t} = \frac{1}{\boldsymbol{Y}^{\mathrm{T}}\boldsymbol{C}_i}, \boldsymbol{e} = \boldsymbol{E}\boldsymbol{t}, \boldsymbol{c}_i = \boldsymbol{C}_i\boldsymbol{t} \tag{21}$$

The linearized model is outlined as follows:

$$\begin{aligned} &\max \boldsymbol{x}^{\mathrm{T}}\boldsymbol{e} \\ &\text{s.t. } \boldsymbol{x}^{\mathrm{T}}\boldsymbol{e} \leqslant 1 \\ &\boldsymbol{y}^{\mathrm{T}}\boldsymbol{c}_i = 1 \end{aligned} \tag{22}$$

Further analysis is based on the solution of the objective function f_i. The ith BS is considered well-configured only when f_i=1; otherwise, the decision-making indices in $\boldsymbol{e}$ are examined and optimized.

Results

Target description

A BS cluster consisting of eight 5G BSs is planned to upgrade the existing 4G BSs in an urban community by MNO, in which eight distributed PVs have already been deployed. The scale of this BS-PV integrated system is detailed in the Supplementary Information. As a comparison, the estimated construction and operation costs of this cluster are over budget under the conventional scheme that BSs have an even distribution geographically, and the states of inner devices are set normally without considering the coupling of the PV cluster. This configuration results in higher costs and lower energy utilization efficiency. Therefore, the proposed two-stage stochastic programming is implemented to optimize the conventional scheme, leveraging the existing PV layout and candidate locations for 5G BSs. The quantum part of the computation is executed on the D-Wave Leap cloud platform, whereas the classical part is carried out on an Intel Core i5-12400 F (2.50 GHz) computer with 16 GB RAM.

In order to capture the inherent variability of PV output and telecom demand, their stochastic characteristics are simulated using representative scenarios. Specifically, historical data on PV power, wireless telecom demand, and meteorological information such as weather and temperature conditions are input together to generate the curves of BS loads and PV outputs across massive sequential scenarios. These scenario-based curves are further clustered and simplified after comparing their probability distribution with the threshold, resulting in 63 typical scenarios after simplification, as shown in Fig. 5. The threshold of 10^{-3} is empirically set to reduce computational burden by excluding scenarios with negligible impact. It is not fixed and can be flexibly adjusted based on the characteristics of different cases.

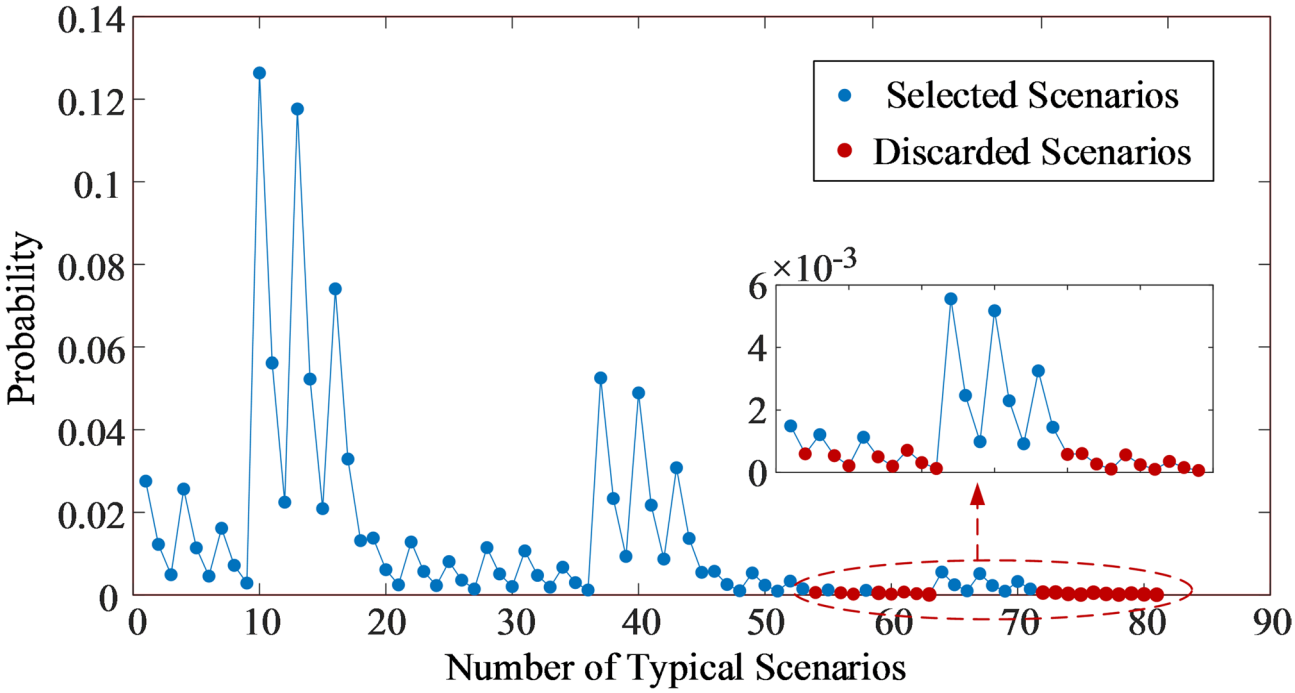

Fig. 5. Probability distribution of typical scenarios. Scenarios with probabilities below 10^{-3} (red dots) are excluded to reduce computational burden. The final model retains 63 typical scenarios (blue dots).

Method	Solution				Cost (p.u.)	Time Consumption (s)
	Location (*x*,*y*)	TD Specification	ES Capacity	AC Mode		
Experience-Oriented	(1,4), (2,2), (4,2), (4,4), (5,6), (6.4), (7,2), (8,6)	2, 2, 1, 2, 3, 1, 3, 2	2, 2, 1, 2, 3, 1, 3, 2	2, 2, 1, 2, 3, 1, 3, 2	2.963	–
Gurobi	(1,6), (2,2), (2,4), (4,1), (4,5), (6.2), (6,5), (8,4)	2, 2, 1, 2, 3, 1, 3, 2	3, 2, 1, 3, 2, 1, 2, 1	2, 3, 1, 3, 3, 2, 2, 1	1.000	1.649
Simulated Annealing	(1,4), (2,2), (2,4), (4,1), (4,5), (6.2), (6,5), (8,4)	2, 2, 1, 2, 3, 1, 3, 2	3, 1, 1, 3, 2, 1, 1, 2	2, 3, 1, 3, 3, 2, 2, 2	1.126	4.193
QA	(1,6), (2,2), (2,4), (4,1), (4,5), (6.2), (6,5), (8,4)	2, 2, 1, 2, 3, 1, 3, 2	3, 2, 1, 3, 2, 1, 2, 1	2, 3, 1, 3, 3, 2, 2, 1	1.000	0.477
WSQA	(1,6), (2,2), (2,4), (4,1), (4,5), (6.2), (6,5), (8,4)	2, 2, 1, 2, 3, 1, 3, 2	3, 2, 1, 3, 2, 1, 2, 1	2, 3, 1, 3, 3, 2, 2, 1	1.000	0.256

Table 3. Comparison of WSQA and benchmark methods in the first-stage deployment

Deployment scheme generated by WSQA

A WSQA is employed to solve the first-stage problem. Its function is evaluated by comparing it with other typical methods. The benchmark methods are selected based on the following four characteristics. Each method is limited to a maximum of 100 iterations, with convergence defined as a relative error of less than 0.5% between consecutive iterations.

(1) Experience-Oriented Planning: The 5G BS cluster is deployed uniformly, with equal distances between all BSs, and the inner device configurations are determined based on experience.
(2) Commercial Solver: The first-stage problem is solved directly using Gurobi.
(3) Heuristic Algorithm: The first-stage problem is solved using Simulated Annealing (SA).
(4) Quantum Algorithm without Warm-Starting: The first-stage problem is solved using QA without considering the warm-starting process.

The comparison of results between WSQA and the above benchmark methods is presented in Table 3. The results show that the deployment scheme obtained by optimization methods presents an obvious reduction of cost, yet Gurobi and Simulated Annealing have their inferiorities in time consumption and solution accuracy. Due to the tunneling effect in the annealing process, quantum-related methods, i.e., QA and WSQA, not only outperform the traditional Gurobi solver in terms of computational efficiency but also achieve a more accurate solution with the lowest cost compared to Simulated Annealing. Furthermore, WSQA further enhances the efficiency of QA with the assistance of warm-starting technology, nearly doubling the performance and achieving a 5.4-fold efficiency improvement compared to the Gurobi solver. As such, WSQA is identified as the method with the best computational performance among those considered. The optimal deployment of the BS cluster is exhibited in Fig. 6.

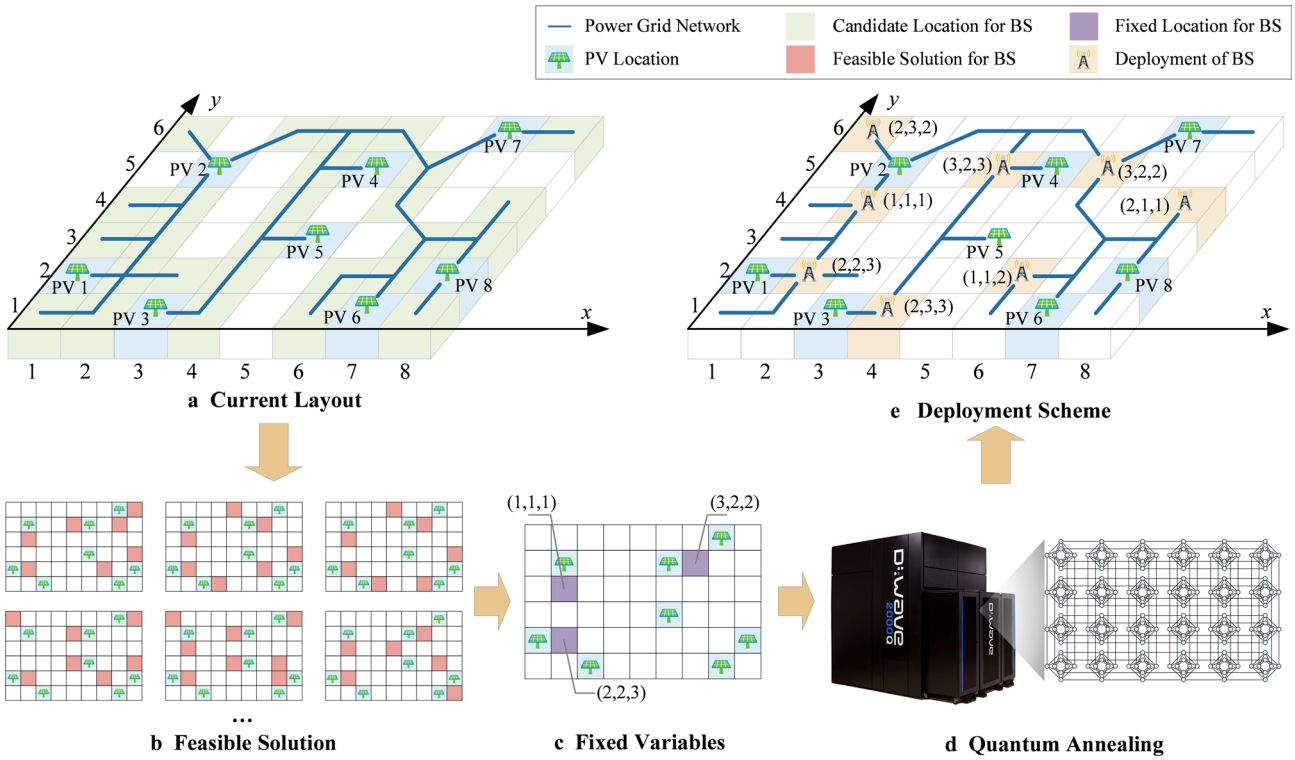

Fig. 6. Workflow for optimal BS cluster deployment. (**a**) Topology of the power grid (solid lines), distribution of PVs (blue squares), and candidate locations for 5G BSs (green squares). (**b**) Feasible solution generated by a classical computer (red squares). (**c**) Variables pre-fixed based on the distribution of the feasible solution (purple squares). (**d**) Remaining variables optimized on the D-Wave quantum annealer. (**e**) Final deployment scheme (yellow squares), each (*a*,*b*,*c*) tuple denotes the TD, ES, and AC configurations.

Furthermore, the convergence speeds of the iterative algorithms (WSQA and Algorithms 2, 3, and 4) are compared to evaluate their performance, as shown in Fig. 7. The results indicate that the annealing-based algorithms (WSQA and Algorithm 4) achieve convergence with fewer iterations and at a faster rate than their counterparts. While Algorithms 2 and 3 generally exhibit a converging trend, their performance fluctuates, with some iterations yielding inferior results to the previous ones, particularly when approaching local optima, where convergence slows significantly. In contrast, annealing-based algorithms demonstrate a consistent improvement in each iteration. Even in the vicinity of local optima, it maintains strong convergence efficiency, owing to its inherent tunneling effect that enables more effective escape from local minima.

Due to the inherent variability in the results of WSQA and Algorithms 3 and 4, a multiple-run strategy is commonly adopted in practice to increase the probability of obtaining the global optimum. Figure 7b compares the best solutions found by the three algorithms across varying numbers of repeated runs. The results clearly show that WSQA can achieve a solution with the required accuracy (or even reach the global optimum) with significantly fewer repetitions. In contrast, SA requires substantially more runs to reach comparable performance, resulting in longer overall computation times in practical applications.

Operation scheme assisted by DEA

Based on the deployment scheme outlined above, DEA is conducted with eight BSs as decision-making units (DMUs). Deviation Index (*DI*), Consistency Index (*CI*), Power Supply Ratios of PVs and the power grid (*PR* and *GR*) are selected as four decision-making indices. Assuming that the 5G BS cluster initially operates under the previous scheme designed for the 4G BS cluster, its operation performance, represented by the cost-effectiveness ratio, is presented in the "Initial State" column of Table 3. Specifically, six of the BSs have objective function values lower than 1, indicating that their respective decision-making indices in the BS-PV integrated urban communities have the following optimization potential:

1) The excessively high values for DI_1, DI_2, DI_3, DI_5, and DI_6 suggest significant deviations between the load curves of the corresponding BS loads and the PV outputs, which is primarily due to the mismatch between PV outputs and ES capacities. Further analysis of the deviation sequence reveals that 68% of the values are negative, even after excluding reasonable deviations caused by the absence of PV outputs at night. Therefore, it is necessary to increase the capacity of the ES units in BS1, BS2, BS3, BS5, and BS6 despite the added maintenance costs.

2) The CI_1, CI_2, CI_3, CI_5, CI_6, and CI_7 are relatively low, indicating poor correlation between the corresponding BSs and the PVs. This suggests frequent instances where BS loads contradict the PV outputs. To address this issue, the switching thresholds for different operating states in the telecom device (TD) and AC units should be lowered, making them more sensitive to variations in predicted PV outputs and telecom demands.

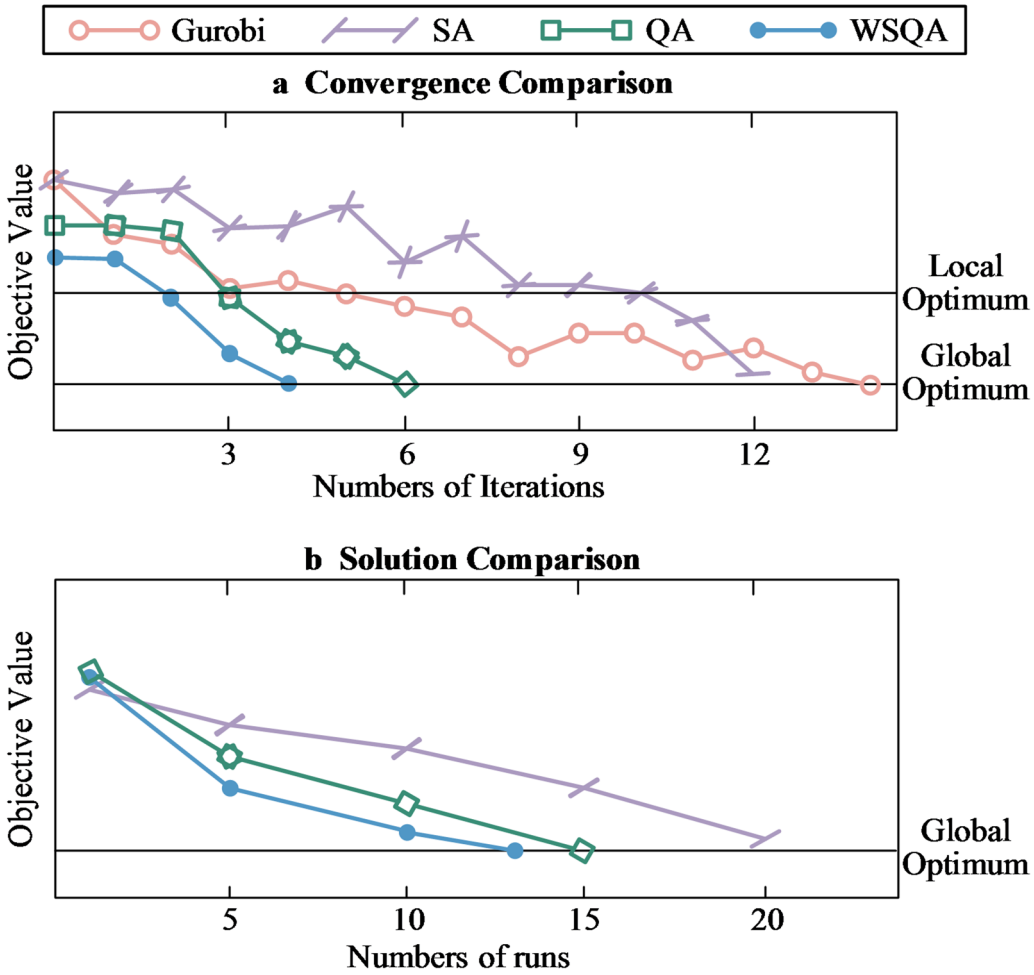

Fig. 7. Performance comparison between WSQA and benchmark methods. Red, purple, green, and blue lines represent Algorithms 2, 3, 4, and WSQA. (**a**) Objective value over iterations. (**b**) Objective value trend across repeated runs.

	Initial state		Optimal solution	
DMUi	f0 i	[DI_i, CI_i, PR_i, GR_i]	f* i	[DI_i, CI_i, PR_i, GR_i]
BS1	0.86	[55.23, 0.59, 0.64, 0.51]	0.98	[51.83, 0.79, 0.84, 0.25]
BS2	0.79	[62.46, 0.46, 0.81, 0.33]	1.00	[49.58, 0.86, 0.81, 0.30]
BS3	0.65	[75.76, 0.47, 0.45, 0.68]	0.97	[52.83, 0.66, 0.76, 0.32]
BS4	1.00	[47.01, 0.85, 0.84, 0.29]	1.00	[47.01, 0.85, 0.84, 0.28]
BS5	0.70	[70.22, 0.61, 0.39, 0.78]	0.99	[51.34, 0.81, 0.83, 0.31]
BS6	0.73	[65.90, 0.42, 0.57, 0.55]	0.98	[50.93, 0.79, 0.78, 0.27]
BS7	1.00	[48.55, 0.82, 0.89, 0.21]	1.00	[48.55, 0.82, 0.89, 0.22]
BS8	0.91	[52.34, 0.66, 0.68, 0.37]	1.00	[52.34, 0.84, 0.86, 0.28]

Table 4. Variation of objective functions and decision-making indices.

3) While PR_2, PR_4, and PR_7 are acceptable, the remaining *PR* values are extremely low, indicating that the PV utilization in parts of the areas is below the requirements. Therefore, the power supply from the PV cluster to BS1, BS3, BS5, BS6, and BS8 should be adjusted to higher values.

4) The *GR* values for BS1, BS3, BS5, BS6, and BS8 exceed the threshold, indicating excessive reliance on the power grid. The high *GR* values align with the low *PR* values to some extent. In addition to the *PR* adjustment, the *GR* can be controlled by increasing ES capacity and optimizing the state-switching thresholds of the AC unit.

The dispatching scheme is iteratively updated to achieve the optimal solutions f^*_i and the respective decision-making indices, as shown in the "Optimal Solution" column of Table 4. Evidently, the objective function of each DMU approaches 1, indicating that the DMU's cost is optimized and the optimal operation performance

has been achieved. Figure 8a shows the power output across all 63 scenarios. Furthermore, four representative scenarios are selected to illustrate the optimal scheduling scheme of BS loads to match PV outputs, as shown in Fig. 8b and e. It is concluded that the scheme of eight BSs varies with both PV outputs and telecom demands. Specifically, the power consumption of TD, ES, and AC remains high to maximize the utilization of PV power in *Scenario 5*. When the telecom demand reduces but PV outputs are maintained at a high level, such as in *Scenario 14*, only the TD power consumption decreases significantly, while ES and AC continue to convert PV power into electricity and cooling as a precaution. *Scenarios 36 and 52* represent conditions with low PV outputs, where both ES and AC are switched to energy-saving modes to reduce the power demand for thermal units. The power consumption of TD is adjusted based on telecom demand, which takes priority over cost-saving considerations in operation.

Furthermore, Fig. 9 compares PV utilization and BS operation costs across 63 scenarios before and after applying the proposed method. The proposed deployment and operation scheme improves PV utilization by 12.53% over the experience-oriented approach, effectively reducing curtailment and associated carbon emissions from conventional energy sources. Moreover, by optimizing energy consumption across TD, ES, and AC components, this case achieves a 51.04% reduction in electricity costs for MNOs.

Discussion

Scalability and broader applicability

Although current quantum computers remain in the NISQ era, and even with the assistance of warm-start techniques, they can only support planning tasks for medium-scale communities. For large-scale urban areas or coupled multi-community scenarios, the original problem must be decomposed into smaller subproblems and solved iteratively, which may lead to a loss in solution accuracy. Nonetheless, the proposed method holds significant promise. As quantum hardware continues to evolve, the WSQA algorithm is expected to exhibit stronger performance due to its integration of variable pre-fixing and warm-starting initialization, as evidenced by the analysis of computational effort. Theoretical analysis of computational time complexity shows that the effort required by the conventional method using Gurobi increases exponentially with the size of the MIP problem, denoted as $O(\exp(N))$, while the complexity of annealing-based quantum algorithms is generally no greater than $O(\exp(\mathrm{sqrt}(N)))$, indicating significantly better scalability. As shown in Fig. 10, quantum algorithms impose a lower computational burden than Gurobi in smaller-scale cases, with this advantage expected to grow even further as quantum annealers evolve and their qubit capacity increases.

Benefits and impacts

Beyond the evident efficiency superiority and methodological feasibility demonstrated in the case study, the proposed method offers several practical and broader implications for stakeholders such as MNO, DNO, and policymakers. By improving photovoltaic resource utilization, the proposed approach aligns with carbon reduction policies and advances the integration of renewable energy into urban energy infrastructures for stakeholders. Meanwhile, the enhanced operational efficiency and significantly reduced planning and operation costs create substantial economic value and improve infrastructure sustainability for operators. These findings closely reflect the original motivation of this study: enabling a mutually beneficial solution for MNOs and DNOs through the coordinated, cost-efficient, and sustainable planning of 5G and PV infrastructures. Moreover,

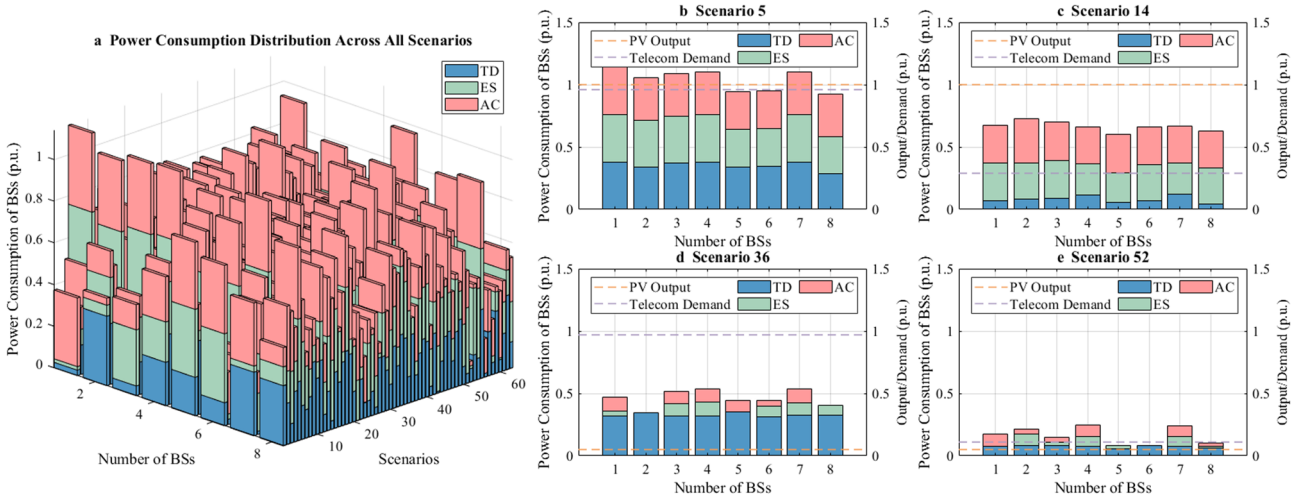

Fig. 8. Optimal operation scheme of the BS-PV integrated urban community. The red and purple curves denote PV output and telecommunication demand; the blue, green, and red bars represent power consumption of TD, ES, and AC, respectively. (**a**) Power Consumption of eight urban BSs under 63 typical scenarios assisted by DEA. (**b**) Scenario 5: High PV output with high telecom demand. (**c**) Scenario 14: High PV output with low telecom demand; (**d**) Scenario 36: Low PV output with high telecom demand. (**e**) Scenario 52: Low PV output with low telecom demand.

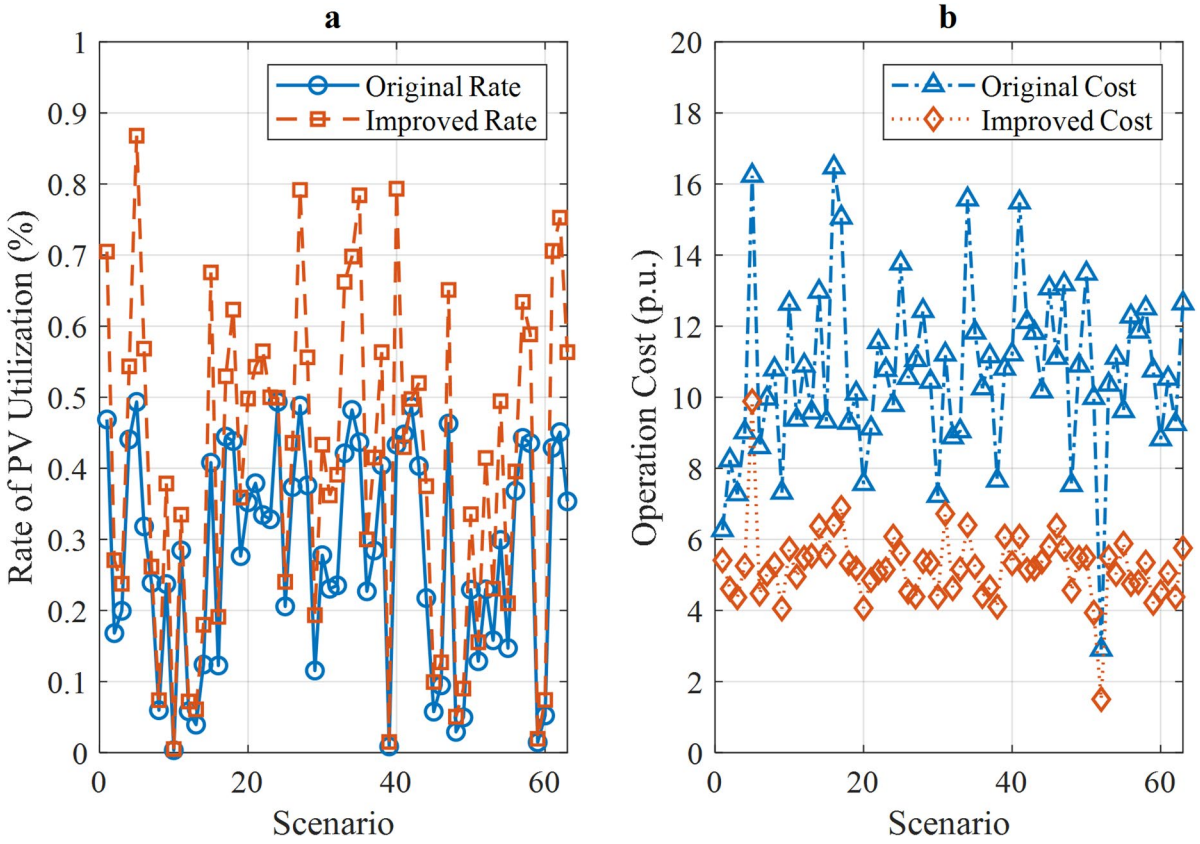

Fig. 9. Comparison of the PV utilization and BS operation costs. (**a**) Comparison of the rate of PV utilization. (**b**) Comparison of the operation costs.

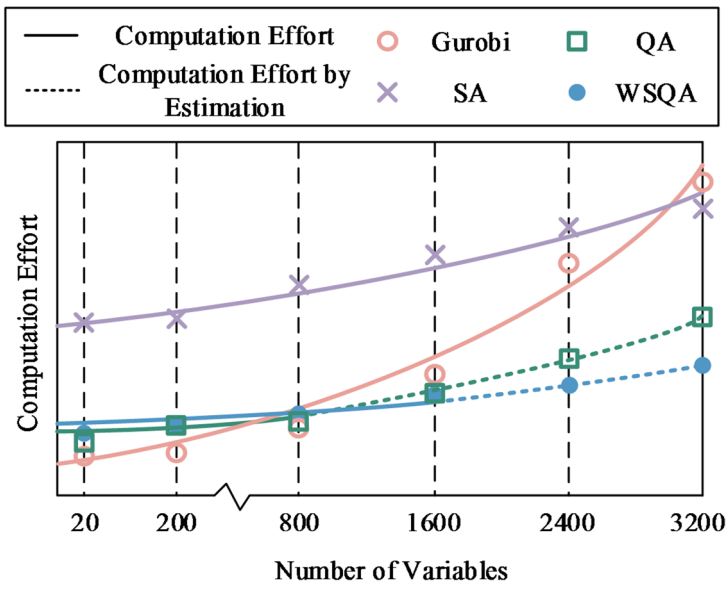

Fig. 10. Comparison of the computational effort in different problem sizes. Compared to QAOA and QA, the WSQA algorithm requires even less computational effort, highlighting its superior scalability.

the modular structure and data-driven nature of our model allow it to be adapted to diverse urban contexts, regulatory environments, and energy mixes, making it applicable across different regions with varying levels of grid maturity and renewable penetration. These broader insights not only validate the robustness of the method but also provide a reference for future interdisciplinary planning frameworks that aim to align digital infrastructure expansion with clean energy goals.

Conclusion

This study proposes a two-stage stochastic programming approach to optimize the co-planning of BS-PV integrated urban communities. The hybrid quantum-classical method performs preliminary deployment of the BS cluster by solving the first-stage problem using WSQA, followed by optimizing the operation scheme according to the operation performance evaluation using DEA. The optimal operation scheme of BS-PV integrated urban communities is generated from maximizing the cost-effectiveness ratio based on DEA, thereby avoiding the optimization of complex nonlinear and spatiotemporal coupled models. The results indicate that the proposed method yields effective deployment and operation schemes, achieving lower costs and higher PV utilization for operators. The contributions are summarized as follows:

1) A hybrid quantum-classical two-stage stochastic programming framework is proposed for co-planning BS-PV integrated urban communities, combining warm-start quantum annealing and DEA to efficiently solve nonlinear, uncertain, and spatiotemporally coupled problems.
2) In a medium-scale urban community case, the method achieves a 5.4× computational speedup and reduces total planning costs to one-third of experience-based strategies.
3) Beyond technical gains, the method promotes renewable energy integration and energy-efficient telecom infrastructure, increasing PV utilization by 12.53%, reducing electricity costs by 51.04%, and contributing to carbon reduction and economic value to operators.

Further research should also consider several hardware- and modeling-related extensions. Firstly, although current quantum annealing platforms address noise and decoherence through repeated sampling strategies, the study does not delve into hardware-level issues, as it primarily targets algorithm-level design. In the near term, before significant hardware advancements, future work could explore algorithmic strategies to mitigate the impact of quantum noise and computational errors. Secondly, the present model assumes fixed PV locations and perfect telecom demand forecasts as reasonable simplifications based on current operational conditions. Relaxing these assumptions and introducing uncertainty in both spatial and temporal variables will enable the model to better capture real-world complexities and enhance its applicability in dynamic urban environments.

Data availability

Data is available from the corresponding author upon reasonable request.

Received: 13 June 2025; Accepted: 30 October 2025
Published online: 28 November 2025

References

1. Al-Dujaili, M. J. & Al-Dulaimi, M. A. Fifth-generation telecommunications technologies: features, architecture, challenges and solutions. *Wirel. Pers. Commun.* **128**, 447–469 (2023).
2. Zhang, S., Liu, N. & Han, J. Temporal and Spatial optimization for 5 g base station groups in distribution networks. *J. Mod. Power Syst. Clean. Energy*. **12**, 1159–1169 (2023).
3. Israr, A., Yang, Q., Li, W. & Zomaya, A. Y. Renewable energy powered sustainable 5 g network infrastructure: opportunities, challenges and perspectives. *J. Netw. Comput. Appl.* **175**, 102910 (2021).
4. Yong, P. et al. Evaluating the dispatchable capacity of base station backup batteries in distribution networks. *Ieee Trans. Smart Grid*. **12**, 3966–3979 (2021).
5. Li, T. et al. Carbon emissions of 5 g mobile networks in China. *Nat. Sustain.* **6**, 1620–1631 (2023).
6. Jiang, H. et al. Globally interconnected solar-wind system addresses future electricity demands. *Nat. Commun.* **16**, 4523 (2025).
7. Hassan, H., Renga, D., Meo, M. & Nuaymi, L. A novel energy model for renewable energy-enabled cellular networks providing ancillary services to the smart grid. *Ieee Trans. Green. Commun. Netw.* **3**, 381–396 (2019).
8. Zeng, B., Zhang, W., Hu, P., Sun, J. & Gong, D. Synergetic renewable generation allocation and 5 g base station placement for decarbonizing development of power distribution system: a multi-objective interval evolutionary optimization approach. *Appl. Energy*. **351**, 121831 (2023).
9. Al, H., Hassan, H., Pelov, A. & Nuaymi, L. Integrating cellular networks, smart grid, and renewable energy: analysis, architecture, and challenges. *Ieee Access.* **3**, 2755–2770 (2015).
10. Ben Rached, N., Ghazzai, H., Kadri, A. & Alouini, M. Energy management optimization for cellular networks under renewable energy generation uncertainty. *Ieee Trans. Green. Commun. Netw.* **1**, 158–166 (2017).
11. Qi, Q., Hou, Z., Liu, X. & Ai, X. An optimal dispatch model for distribution network considering the adaptive aggregation of 5 g base stations. *Int. J. Electr. Power Energy Syst.* **161**, 110170 (2024).
12. Zhuang, H., Chen, J. & Gilimyanov, R. Hierarchical energy optimization with more realistic power consumption and interference models for ultra-dense networks. *Ieee Trans. Wirel. Commun.* **19**, 4507–4518 (2020).
13. Xu, J., Duan, L. & Zhang, R. Energy group buying with loading sharing for green cellular networks. *Ieee J. Sel. Areas Commun.* **34**, 786–799 (2016).
14. Dai, Y. et al. Collaborative optimization of distribution network and 5 g base stations considering its communication load migration and energy storage dynamic backup flexibility. *Int. J. Electr. Power Energy Syst.* **160**, 110124 (2024).
15. Renga, D., Hassan, H. A. H., Meo, M. & Nuaymi, L. Energy management and base station on/off switching in green mobile networks for offering ancillary services. *Ieee Trans. Green. Commun. Netw.* **2**, 868–880 (2018).
16. Li, K. et al. Distributed stochastic scheduling of massive backup batteries in cellular networks for operational reserve and frequency support ancillary services. *J. Mod. Power Syst. Clean. Energy*. **12**, 393–404 (2023).
17. Hui, H. et al. 5 g network-based internet of things for demand response in smart grid: a survey on application potential. *Appl. Energy*. **257**, 113972 (2020).

18. Han, J., Liu, N., Huang, Y. & Zhou, Z. Collaborative optimization of distribution network and 5 g mobile network with renewable energy sources in smart grid. *Int. J. Electr. Power Energy Syst.* **130**, 107027 (2021).
19. Zhang, X. et al. Optimal capacity planning and operation of shared energy storage system for large-scale photovoltaic integrated 5 g base stations. *Int. J. Electr. Power Energy Syst.* **147**, 108816 (2023).
20. Nourollahi, R., Akbari-Dibavar, A., Agabalaye-Rahvar, M., Zare, K. & Anvari-Moghaddam, A. Hybrid robust-cvar optimization of hybrid ac-dc microgrid. In *proceedings of the 11th Smart Grid Conference (SGC)* 1-52021 (2021).
21. Salyani, P., Nourollahi, R., Zare, K. & Razzaghi, R. A new Milp model of switch placement in distribution networks with consideration of substation overloading during load transfer. *Sustainable Energy Grids Networks*. **32**, 100944 (2022).
22. Dongjuan, M. et al. Research on decentralized resource operation optimization of virtual power plant with 5 g base station. *Int J. Low-Carbon Technol* (2024).
23. Ganame, H., Yingzhuang, L., Ghazzai, H. & Kamissoko, D. 5 g base station deployment perspectives in millimeter wave frequencies using meta-heuristic algorithms. *Electronics* **8**, 1318 (2019).
24. Han, J., Liu, N. & Catalão, P. S. Optimization of distribution network and mobile network with interactive balance of flexibility and power. *Ieee Trans. Power Syst.* **38**, 2512–2524 (2023).
25. Abuelrub, A., Awwad, B. & Al-Masri, H. M. K. Solving wind-integrated unit commitment problem by a modified African vultures optimization algorithm. *Iet Generation Transmission Distribution*. **17**, 3678–3691 (2023).
26. Abuelrub, A., Al-Masri, M. K. & Singh, C. H. Techno-economic investigation of a hybrid wind-solar distribution system using stochastic optimization. In *proceedings of the North American Power Symposium (NAPS)*, 1-62019)., 1-62019). (2019).
27. Abuelrub, A., Saadeh, O. & Al-Masri, H. M. K. Scenario aggregation-based grid-connected photovoltaic plant design. *Sustainability* **10**, 1275 (2018).
28. Nourollahi, R., Nojavan, S. & Zare, K. in *Electricity Markets: New Players and Pricing Uncertainties*, edited by Nojavan, S. & Zare, KSpringer International Publishing, Cham,. pp. 135–168. (2020).
29. Ling, J., Zhang, Q., Geng, G. & Jiang, Q. Hybrid quantum annealing decomposition framework for unit commitment. *Electr. Power Syst. Res.* **238**, 111121 (2025).
30. Hong, W., Xu, W. & Teng, F. Qubit-efficient quantum annealing for stochastic unit commitment. Arxiv Preprint Arxiv:2502.15917 (2025).
31. Silva, F. F. C., Carvalho, P. M. S. & Ferreira, L. A. F. M. A quantum computing approach for minimum loss problems in electrical distribution networks. *Sci. Rep.* **13**, 10777 (2023).
32. Shao, Y. et al. Quantum-enabled topological optimization of distributed energy storage for resilient black-start operations. *Sci. Rep.* **15**, 18034 (2025).
33. Wei, X. et al. Hybrid quantum–classical benders' decomposition for federated learning scheduling in distributed networks. *Ieee Trans. Netw. Sci. Eng.* **11**, 6038–6051 (2024).
34. Hosseina, M., Moghaddam, M. S. & Hassannia, A. Optimizing energy and load management in Island microgrids for enhancing resilience against resource interruptions. *Sci. Rep.* **15**, 16297 (2025).
35. Quinton, F. A., Myhr, P. A. S., Barani, M., Del Granado, C., Zhang, H. & P. & Quantum annealing applications, challenges and limitations for optimisation problems compared to classical solvers. *Sci. Rep.* **15**, 12733 (2025).
36. Nakamura, S. et al. Efficiency score from data envelopment analysis can predict the future onset of hypertension and dyslipidemia: a cohort study. *Sci. Rep.* **9**, 16309 (2019).
37. Asfora, B. A., Banfi, J. & Campbell, M. Mixed-integer linear programming models for multi-robot non-adversarial search. *Ieee Robot Autom. Lett.* **5**, 6805–6812 (2020).
38. Kim, S. et al. Quantum annealing for combinatorial optimization: a benchmarking study. *Npj Quantum Inf.* **11**, 77 (2025).
39. Qi, W. A. et al. Optimizing the ultra-dense 5 g base stations in urban outdoor areas: coupling Gis and heuristic optimization. *Sust Cities Soc.* **63**, 102445 (2020).
40. Willsch, D. et al. Benchmarking advantage and d-wave 2000q quantum annealers with exact cover problems. *Quantum Inf. Process.* **21**, 141 (2022).
41. Abel, S., Blance, A. & Spannowsky, M. Quantum optimization of complex systems with a quantum annealer. *Phys. Rev. A*. **106**, 42607 (2022).
42. Li, Y. et al. Practical twin-field quantum key distribution parameter optimization based on quantum annealing algorithm. *Quantum Sci. Technol.* **9**, 45050 (2024).
43. Li, R. Y., Di Felice, R., Rohs, R. & Lidar, D. A. Quantum annealing versus classical machine learning applied to a simplified computational biology problem. *Npj Quantum Inf.* **4**, 14 (2018).
44. Glos, A., Krawiec, A. & Zimborás, Z. Space-efficient binary optimization for variational quantum computing. *Npj Quantum Inf.* **8**, 39 (2022).
45. Morstyn, T. Annealing-based quantum computing for combinatorial optimal power flow. *Ieee Trans. Smart Grid*. **14**, 1093–1102 (2023).
46. Atobe, Y., Tawada, M. & Togawa, N. Hybrid annealing method based on Subqubo model extraction with multiple solution instances. *Ieee Trans. Comput.* **71**, 2606–2619 (2021).
47. Tate, R., Farhadi, M., Herold, C., Mohler, G. & Gupta, S. Bridging classical and quantum with Sdp initialized warm-starts for Qaoa. *Acm Trans. Quantum Comput.* **4**, 1–39 (2023).
48. Liu, J., Shao, L., Jin, F. & Tao, Z. A multi-attribute group decision-making method based on trust relationship and Dea regret cross-efficiency. *Ieee Trans. Eng. Manage.* **71**, 824–836 (2022).
49. Wang, R., Li, D. & Yu, G. Research on bilateral matching decision method considering attribute association in heterogeneous information environment. *J. Intell. Fuzzy Syst.* **38**, 4779–4792 (2020).
50. Camanho, A. S., Silva, M. C., Piran, F. S. & Lacerda D. P. A literature review of economic efficiency assessments using data envelopment analysis. *Eur. J. Oper. Res.* **315**, 1–18 (2024).
51. Lee, J. & Kim, J. Are electric vehicles more efficient? A slacks-based data envelopment analysis for European road passenger transportation. *Energy* **279**, 128117 (2023).

Acknowledgements

This work was supported by the National Natural Science Foundation of China (52477132).

Author contributions

Y. X. executed the experiments and wrote the initial manuscript draft. Z. L. conceived the study, designed the experiments, and revised the manuscript. X. H. and R. L. assisted in the revision and polishing of the manuscript. All authors read and approved the final manuscript.

Funding

This work was supported by the National Natural Science Foundation of China (52477132).

Declarations

Competing interests
The authors declare no competing interests.

Additional information
Supplementary Information The online version contains supplementary material available at https://doi.org/10.1038/s41598-025-26699-2.

Correspondence and requests for materials should be addressed to Z.L.

Reprints and permissions information is available at www.nature.com/reprints.

Publisher's note Springer Nature remains neutral with regard to jurisdictional claims in published maps and institutional affiliations.